Spectral-scaling-based extension to the attached eddy model of wall turbulence

Dileep Chandran, * Jason P. Monty, and Ivan Marusic
Department of Mechanical Engineering, University of Melbourne, Victoria 3010, Australia

(Received 19 May 2020; accepted 18 September 2020; published 16 October 2020)

Two-dimensional (2D) spectra of the streamwise velocity component, measured at friction Reynolds numbers ranging from 2400 to 26 000, are used to refine a model for the logarithmic region of turbulent boundary layers. Here we focus on the attached eddy model (AEM). The conventional AEM assumes the boundary layer to be populated with hierarchies of self-similar wall-attached (Type A) eddies alone. While Type A eddies represent the dominant energetic large-scale motions at high Reynolds numbers, the scales that are not represented by such eddies are observed to carry a significant proportion of the total kinetic energy. Therefore, in the present study, we propose an extended AEM that incorporates two additional representative eddies. These eddies, named Type C_A and Type SS, represent the self-similar but wall-incoherent low-Reynolds-number features and the non-self-similar wall-coherent superstructures, respectively. The extended AEM is shown to better predict a greater range of energetic length scales and capture the low- and high-Reynolds-number scaling trends in the 2D spectra of all three velocity components. A discussion on spectral self-similarity and the associated k^{-1} scaling law is also presented.

DOI: 10.1103/PhysRevFluids.5.104606

I. INTRODUCTION

The logarithmic region, or the inertial sublayer, is the most important region within a turbulent boundary layer at high Reynolds number, owing to its significant contribution to the overall production of turbulent kinetic energy [1,2]. The importance of this inertia-dominated region has motivated several studies to characterize the coherent energy-containing motions, or "eddies," that reside within this region of the boundary layer [2–8]. It is the notion of self-similarity of such eddies that underpins a number of models for the logarithmic region of wall-bounded turbulent flows. Among such models, those that are based on the attached eddy hypothesis of Townsend [9] have gained significant popularity (see Refs. [10–20], among others).

The attached eddy hypothesis assumes the boundary layer as a random distribution of "persistent, organized flow patterns" that are influenced by the wall and whose size scales with distance from the wall. Based on the hypothesis, Perry and Chong [21] developed an attached eddy model (AEM) by prescribing physical shapes to the self-similar structures. The key feature of the AEM is the concept of a "representative attached eddy" and the boundary layer is modeled as an assemblage of discrete but self-similar hierarchies of such eddies. Following Townsend's hypothesis [9], the size and population density of the eddies are directly and inversely proportional to their distance from the wall, respectively. Further, based on dimensional analysis, Perry and Chong [21] reported such hierarchies of geometrically self-similar eddies, over a range of length scales, to contribute equally to the premultiplied turbulent kinetic energy. The authors hence proposed a k_x^{-1} scaling in the one-dimensional (1D) energy spectra as a characteristic of self-similarity. Here k_x is the streamwise wave

*dileep.padinjare@unimelb.edu.au

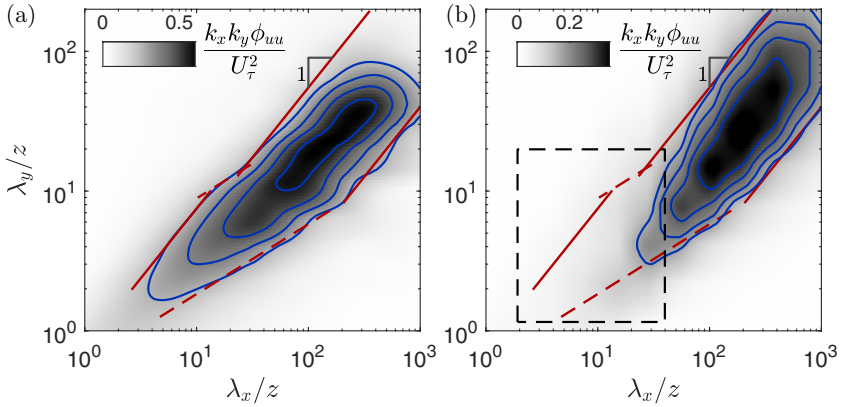

FIG. 1. (a) Two-dimensional spectrum of the streamwise velocity (u) at $z^+ = 2.6\mathrm{Re}_\tau{}^{1/2}$ for $\mathrm{Re}_\tau \approx 26\,000$; the blue contour lines represent $k_x k_y \phi_{uu}/U_\tau^2 = 0.25,\ 0.35$, and 0.45. (b) 2D spectrum obtained from attached eddy model with Type A eddies at same z^+ and Re_τ. The red solid and dashed lines denote the $\lambda_y/z \sim \lambda_x/z$ scaling and $\lambda_y/z \sim (\lambda_x/z)^{1/2}$ relationship, respectively.

number. A refinement to the Perry and Chong model was made by Perry *et al.* [22] where the discrete hierarchical organization was replaced with a continuous distribution of eddies, whose sizes varied from 100 viscous units to the order of boundary layer thickness. Following that, several refinements were made to the AEM based on experimental observations in order to better predict the Reynolds stresses, energy spectra, structure functions, and higher-order moments (e.g., Refs. [12,23–28]). A comprehensive review of the AEM and the various refinements made to the model to date is provided by Marusic and Monty [29].

Insights on the three-dimensional geometry of self-similar eddies in turbulent boundary layers have been obtained from recent high-Reynolds-number multipoint measurements. Baars *et al.* [30] studied spectral coherence of synchronous near-wall and outer-region velocity signals and reported that the structures that are coherent with the wall have a streamwise—wall-normal aspect ratio of $\lambda_x/z \approx 14$. Here λ_x and z denote streamwise wavelength and wall-normal distance, respectively. Chandran *et al.* [31] conducted two-point measurements of streamwise velocity (u) in the streamwise—spanwise plane in order to compute the 2D spectra as a function of streamwise and spanwise wavelengths, λ_x and λ_y, respectively. At high Reynolds numbers, they observed that the smaller length scales retained the low-Reynolds-number behavior with a nominal $\lambda_y/z \sim (\lambda_x/z)^{1/2}$ relationship between the streamwise and spanwise length scales. In contrast, the larger length scales [$\lambda_x, \lambda_y > \mathcal{O}(10z)$] were observed to transition toward a $\lambda_y/z \sim \lambda_x/z$ scaling that is representative of self-similarity. They reported that the self-similar large scales have a streamwise—spanwise aspect ratio of $\lambda_x/\lambda_y \approx 7$ and their streamwise—wall-normal aspect ratio agreed with that of the wall-coherent motions of Baars *et al.* [30]. More recently, Baidya *et al.* [32] extended the model of Baars *et al.* [30] by also capturing the azimuthal or spanwise information of wall-coherent structures in pipe and boundary layer flows at high Reynolds numbers and reported the self-similar structures to follow an aspect ratio of 7:1:1 in the streamwise, spanwise, and wall-normal directions, respectively.

Adopting the empirically observed aspect ratio of self-similar eddies, Chandran *et al.* [31] showed that hierarchies of self-similar wall-attached eddies, named Type A (following the notation of Marusic and Perry [23]), represented the energetic large-scale region of the 2D spectrum reasonably well. This result is reviewed in Fig. 1, where the 2D spectrum obtained from the AEM is compared against the experimental data at a friction Reynolds number of $\mathrm{Re}_\tau = 26\,000$ at $z^+ = 2.6\mathrm{Re}_\tau{}^{1/2}$, corresponding to the start of the logarithmic region [33]. (Here $\mathrm{Re}_\tau = \delta U_\tau/\nu$ and $z^+ = zU_\tau/\nu$, where δ is the boundary layer thickness, U_τ is the friction velocity, and ν is the

kinematic viscosity.) The model, however, does not capture the entire range of energetic scales that is observed experimentally. For example, Fig. 1 shows that the smaller-scale region of the 2D spectrum which followed an empirically observed $\lambda_y/z \sim (\lambda_x/z)^{1/2}$ relationship is not modeled [region within the black dashed box in Fig. 1(b)]. Based on the recent high-Reynolds-number 2D cross-spectrum data of Deshpande *et al.* [34], it was observed that Type A eddies model the energetic scales in the logarithmic region that have a finite correlation at the wall. Their results suggest that the smaller scales unresolved by Type A eddies are mostly wall incoherent. This is, they do not physically extend or have a correlation with the viscous near-wall region. Furthermore, the model also omits the contribution from the non-self-similar, very large scale attached motions [19,35,36] that are characteristic of the superstructures in turbulent boundary layers.

The significance of these energetic scales that are unresolved by the attached eddy model is emphasized in the recent investigations by Baars and Marusic [35,36]. Their studies employ spectral-coherence-based filters to decompose the measured streamwise turbulent kinetic energy into three spectral subcomponents: a wall-incoherent high-wave-number component and two wall-coherent lower-wave-number components. The two wall-coherent subcomponents represent the self-similar structures in the context of the attached eddy hypothesis and the non-self-similar very large-scale motions. The authors report that a k_x^{-1} scaling in the 1D streamwise spectra and the corresponding log-law in the streamwise turbulent intensity profile [37], both indicative of self-similarity, would be masked (for $\mathrm{Re}_\tau \lesssim 80\,000$) due to the overlap of the subcomponent energies. Hence, at any practically encountered Reynolds number, a discussion of spectral self-similarity based on the attached eddy model is incomplete when only considering the Type A spectral component.

Accordingly, the objective of the current study is to extend the attached eddy model by identifying and incorporating into the conventional AEM (i) the representative energetic small-scale structures that are incoherent with the wall and (ii) the representative very large scale motions (or global modes) that are characteristic of the superstructures in turbulent boundary layers. To this end, based on the scaling of experimental 2D spectra of u for friction Reynolds numbers ranging from 2400 to 26 000, the significant spectral subcomponents are identified in Sec. II. The extension of the AEM is discussed in Sec. III and the results are compared against the experiments in Sec. IV. Finally, a discussion on spectral self-similarity based on the extended attached eddy model is carried out in Sec. V. It is noted that throughout this paper, superscript "+" indicates normalization by viscous length and velocity scales, ν/U_τ and U_τ, respectively. The streamwise, spanwise, and wall-normal directions are denoted by x, y, and z, respectively, and u, v, and w denote the respective fluctuating velocity components.

II. SCALING OF EXPERIMENTAL 2D SPECTRA

The extension of the AEM discussed in this paper is driven by the scaling of 2D spectra of u, measured from low ($\mathrm{Re}_\tau = 2400$) to high ($\mathrm{Re}_\tau = 26\,000$) Reynolds numbers. These measurements were conducted in the low-Re open-return boundary layer wind tunnel [38] and the high-Re boundary layer wind tunnel [39] facilities, respectively, at the University of Melbourne. The 2D correlations of u, and subsequently the 2D spectra of u, were computed using synchronous two-point hot-wire measurements. Reference [31] provides full details of the experimental set-ups and measurement technique, as they are not included here for brevity.

Figures 2(a) and 2(c) show the inner- and outer-flow scalings [22], respectively, of a contour of constant energy ($k_x k_y \phi_{uu}/U_\tau^2 = 0.15$) of the 2D spectra as a function of λ_x and λ_y. A constant energy contour shows the spectrum of streamwise and spanwise length scales that contribute equally to the turbulent kinetic energy. Their inner- and outer-flow scaling arguments are probed by normalizing λ_x and λ_y with the wall height (z) and the boundary layer thickness (δ), respectively. Similarly, Figs. 2(b) and 2(d) show the inner- and outer-flow scalings, respectively, of the energetic ridges of the 2D spectra. The energetic ridge is computed as the maximum value of $k_x k_y \phi_{uu}/U_\tau^2$ corresponding to each streamwise wavelength, λ_x. The energetic ridge therefore indicates the aspect ratios (λ_x/λ_y) of the dominant energy carrying structures at a given wall height and can hence be used as a tool

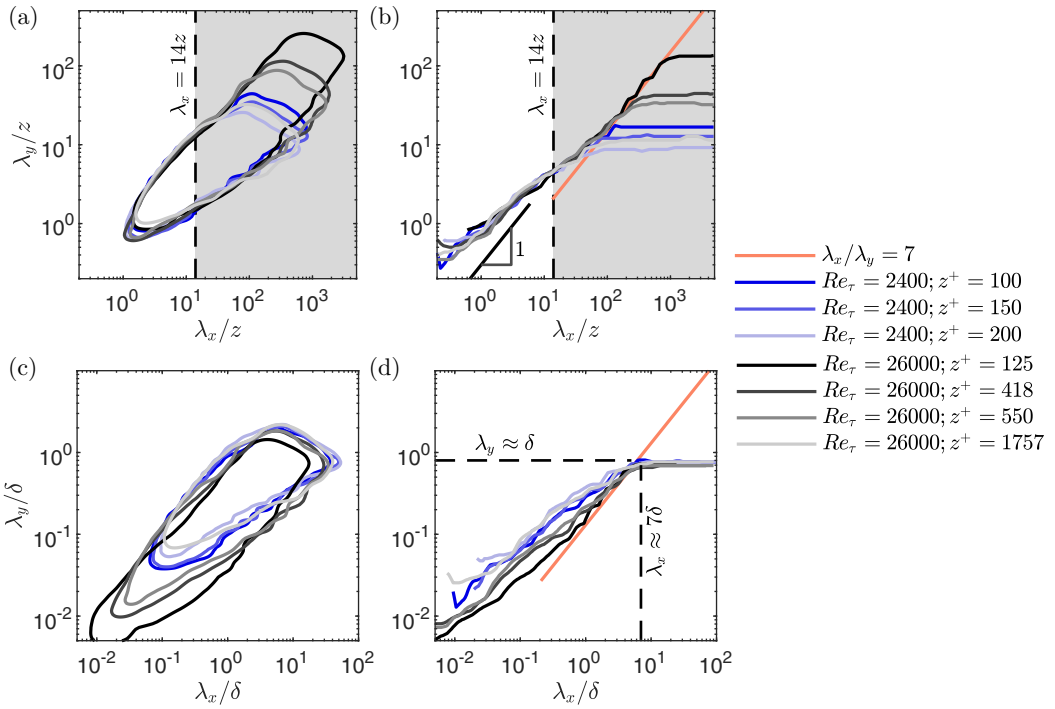

FIG. 2. [(a) and (c)] Inner-flow scaling and outer-flow scaling, respectively, of the constant energy contour $k_x k_y \phi_{uu}/U_\tau^2 = 0.15$, and [(b) and (d)] inner-flow scaling and outer-flow scaling, respectively, of the energetic ridges. The shaded regions in (a) and (b) represents the wall-coherent scales as per Baars *et al.* [30]. The boundary layer thicknesses δ at $\mathrm{Re}_\tau = 2400$ and 26 000, calculated by fitting the velocity profile to the composite profile of Chauhan *et al.* [41], are 0.069 m and 0.337 m, respectively, and the friction velocities U_τ at $\mathrm{Re}_\tau = 2400$ and 26 000 are 0.545 m/s and 1.231 m/s, respectively.

to observe geometric self-similarity [31,40]. The various scaling laws of these energetic contours and ridges, at different wall heights and Reynolds numbers, are inspected in order to prescribe the geometry and organization of the various representative eddies in the extended AEM.

A. Wall-coherent self-similar motions

Following the definition provided by Baars *et al.* [30], wall-coherent structures in the outer region are portions of velocity fluctuations which correlate with the velocity fluctuations very close to the wall (or the wall-shear stress signature). Baars *et al.* [30] isolates these wall-coherent scales from the broadband turbulence by employing an empirical filter that is based on 1D spectral coherence (as a function of λ_x). They observed that the structures coherent with the wall have streamwise wavelengths $\lambda_x > 14z$. These scales are represented by the dark-shaded region in Figs. 2(a) and 2(b). Note that identifying the exact boundaries of the wall-coherent region in a 2D spectrum would require a 2D spectral-coherence-based filter obtained as a function of both λ_x and λ_y. Hence the dark-shaded region is only an approximate reference for the wall-coherent scales, and some of the very small and the very large spanwise length scales within this region are likely incoherent with the wall. As discussed by Chandran *et al.* [31], the wavelengths of the large scales [$\lambda_x, \lambda_y > \mathcal{O}(10z)$, hereafter referred to as the *large-eddy region*] tend to obey a relationship of $\lambda_y/z \sim (\lambda_x/z)^m$, where the value of m approaches unity at high Reynolds numbers or as the measurement location is moved closer to the wall (for $z \gg \nu/U_\tau$). It can be observed from the inner-flow scaling of the ridges [Fig. 2(b)] that the aspect ratio of such dominant large-scale structures that tend toward

self-similarity with $m = 1$ is $\lambda_x/\lambda_y \approx 7$. These large-scale self-similar structures that are coherent with the wall are consistent with eddies described in Townsend's attached eddy hypothesis. Additionally, when the wavelengths are scaled in δ as shown in Fig. 2(d), the ridges collapse at $\lambda_x \approx 7\delta$ and $\lambda_y \approx \delta$ resulting in the same aspect ratio of $\lambda_x/\lambda_y \approx 7$. Therefore, the largest wall-attached self-similar structures have a characteristic "length" and "width" of roughly 7δ and 1δ in spectral space. These dimensions also agree with the observations of Baidya *et al.* [32], where they found that a self-similar eddy has an aspect ratio of 7:1:1 in the x, y, and z directions, respectively.

B. Wall-coherent non-self-similar very large scale motions

From Fig. 2(d) we observe that the large scales nominally grow self-similarly, i.e., $\lambda_y \sim \lambda_x$, until $\lambda_x \approx 7\delta$ and $\lambda_y \approx \delta$. Beyond these limits, the ridge trends toward larger streamwise wavelengths while maintaining a constant spanwise width of $\lambda_y \approx \delta$ and with the energy dropping. At these very large scales, a good collapse of the ridges is observed with outer-flow scaling, irrespective of Reynolds number. This agrees with the findings of Tomkins and Adrian [42] that the structures with the largest streamwise wavelengths organize with a spanwise spacing of $\lambda_y = 0.75\delta$–0.9δ. This spanwise spacing is also consistent with the width of the anticorrelations of streamwise velocity in the spanwise direction observed by Hutchins and Marusic [5]. They reported that such events tend to have long streamwise correlations; a characteristic typical of "superstructures" in boundary layer flows. It can be noted from Figs. 2(a) and 2(b) that these outer-scaled length scales do not follow a self-similar scaling with z. These structures are hence observed to be consistent with the "global" modes of del Álamo and Jiménez [43], and the "wall-attached non-self-similar" motions of Hwang and Sung [15] and Yoon *et al.* [19], that extend deep in the wall-normal direction. It is also noted that even though the energetic ridges exhibit a good collapse in outer scaling for $\lambda_x > 7\delta$ [Fig. 2(d)], the constant energy contours [Fig. 2(c)] collapse only within the logarithmic region ($2.6\mathrm{Re}_\tau^{1/2} \leqslant z^+ \leqslant 0.15\mathrm{Re}_\tau$). The contour corresponding to $\mathrm{Re}_\tau = 26000$ and $z^+ = 125(< 2.6\mathrm{Re}_\tau^{1/2})$ does not seem to follow an energetic similarity. This trend is expected based on the findings of Baars and Marusic [35], who showed that the energy contributed by the very large scale structures that are coherent with the wall is roughly constant for $2.6\mathrm{Re}_\tau^{1/2} \leqslant z^+ \leqslant 0.15\mathrm{Re}_\tau$ and reduces for $z^+ < 2.6\mathrm{Re}_\tau^{1/2}$.

C. Wall-incoherent wall-scaled motions

According to Baars *et al.* [30], wall-incoherent motions are characterized by a streamwise—wall-normal aspect ratio of $\lambda_x/z < 14$ and correspond to the unshaded region in Figs. 2(a) and 2(b). In agreement with recent studies [19,35,36,44], the contribution of wall-incoherent structures to the turbulent kinetic energy, which is the area within the 2D spectra in the unshaded region in Fig. 2(a), appears to be significant. Even though important across the Reynolds-number range studied here, the relative energy contribution of these wall-incoherent structures is observed to be more significant at low Reynolds number. Interestingly, as seen in Fig. 2(a), the wall-incoherent region of the 2D spectra appears to follow a clear inner-flow scaling except for the very small Kolmogorov-type scales. This suggests the existence of wall-detached energetic motions whose characteristic lengths scale with distance from the wall. Moreover, the collapse of the constant energy contours suggests an invariant inner-flow scaled contribution of these wall-incoherent wall-scaled motions to the turbulent kinetic energy for all wall locations and Reynolds numbers considered here. Now if we focus on the inner-flow scaling of the energetic ridges in this regime [Fig. 2(b)], then a good collapse is observed and the ridges follow a $\lambda_y \sim \lambda_x$ behavior at these smaller scales [$\lambda_x, \lambda_y \sim \mathcal{O}(z)$], resulting in an aspect ratio of $\lambda_x/\lambda_y \approx 1$. Such a linear relationship at the scales $\mathcal{O}(z)$ was also reported by del Álamo *et al.* [40]. Hence, at high Reynolds number, the empirically observed $\lambda_y/z \sim (\lambda_x/z)^{1/2}$ relationship (that was predominant at low Reynolds numbers) bridges the two $\lambda_y \sim \lambda_x$ relationships observed at smaller [$\lambda_x, \lambda_y \sim \mathcal{O}(z)$] and larger [$\lambda_x, \lambda_y > \mathcal{O}(10z)$] length scales.

III. EXTENDED ATTACHED EDDY MODEL

In the previous section, we identified three major contributors to the turbulent kinetic energy based on spectral-scaling arguments: (i) wall-coherent self-similar motions, (ii) wall-coherent very large scale motions, and (iii) wall-incoherent but wall-scaled small-scale motions. Here we attempt to extend the attached eddy model by assigning a representative structure and an organization to each of the above identified subcomponents and name them as Type A, Type SS, and Type C_A eddies, respectively. Following prior experimental observations [45–47] and for simplicity, we model the Type A, Type SS, and Type C_A representative structures using packet eddies, where hairpins at various stages of their self-similar growth are aligned in the streamwise direction [24,48]. In the present study, the packets are formed by aligning geometrically scaled "Λ hairpins" in the streamwise direction at a growth angle of 10° [46] for all three representative structures. The spacing between the hairpins are fixed for all three packet eddies and is equal to $0.1\,\mathcal{H}$, where $\mathcal{H}$ is the height of the eddy [Fig. 3(a)]. Each individual Λ hairpin within a packet is constructed using two vortex rods with a characteristic radius of $0.02\,\mathcal{H}$, and the no-penetration condition at the wall is enforced by supplementing each vortex rod with its own mirror image at the wall. The height of the largest eddy is δ_E, which is of the order of boundary layer thickness. The length ($\mathcal{L}$) and the maximum width ($\mathcal{W}$) of the representative packet eddies are chosen to match the aspect ratios of the dominant motions identified based on the scaling of 2D spectra from experiments in Sec. II. Consequently, the values of $[\mathcal{L}/\mathcal{H}, \mathcal{W}/\mathcal{H}]$ prescribed for Type A, Type SS, and Type C_A eddies are [3.5, 0.5], [4, 0.3], and [1, 1], respectively. (Monty *et al.* [49] has demonstrated the effect of varying the aspect ratio of the representative eddy, $\mathcal{L}/\mathcal{W}$, on the computed 2D spectrum.) No other shapes for hairpins are considered in the present study as the objective is to understand the scaling of representative packet eddies rather than focusing on the exact form of individual hairpins. The organization of Type A, Type C_A, and Type SS eddies in the boundary layer is illustrated in Figs. 3(b) to 3(d), respectively. The results obtained with Type A, Type C_A, and Type SS structures are respectively color-coded using shades of red, blue, and green, and the results from the composite model are represented with shades of gray.

A. Type A

Type A eddies represent the wall-attached self-similar motions as conceptualized by Townsend [9] and discussed in Sec. II A. The geometry of the representative packet [$\mathcal{L}$ and $\mathcal{W}$, as illustrated in Fig. 3(a)] is chosen such that the aspect ratio, $\mathcal{L}/\mathcal{W}$, is equal to the average aspect ratio of the wall-coherent self-similar motions observed in the experiments, which is $\lambda_x/\lambda_y \approx 7$. The boundary layer is then populated with hierarchies of representative packet eddies that belong to different stages of their self-similar growth [22]. For illustrative purposes, Fig. 3(b) represents a discrete model with four different hierarchies of Type A eddies; the wall-normal extent of the largest and the smallest eddies in the schematic being $\delta_E (\sim \mathcal{O}(\delta))$ and $\delta_E/2^3$, respectively. The curved boxes [in Figs. 3(b)–3(d)] are illustrative of a cross-stream slice of the velocity field (y-z plane) from the representative eddies and do not in any form represent the actual velocity field. Figure 3(b) is similar to the physical model of Perry *et al.* [22] where the streamwise and spanwise extents of the representative eddies scale with distance from the wall (z) and their probability density is inversely proportional to z. However, it should be noted that unlike in Fig. 3(b), the actual simulation assumes a continuous hierarchy of eddies with the heights of the largest and the smallest eddies being $\mathcal{H}_L = \delta_E$ and $\mathcal{H}_S^+ = 100$, respectively. Hence, following Perry *et al.* [22], the 2D spectra resulting from this random distribution of self-similar eddies is computed as:

$$\frac{\phi_{uu}\left(k_x\mathcal{H}, k_y\mathcal{H}, \frac{z}{\mathcal{H}_L}, \frac{z}{\mathcal{H}_S}\right)}{U_\tau^2} = \int_{\mathcal{H}_S}^{\mathcal{H}_L} \frac{\Phi_{uu}\left(k_x\mathcal{H}, k_y\mathcal{H}, \frac{z}{\mathcal{H}}\right)}{U_\tau^2} \mathcal{P}(\mathcal{H})\mathrm{d}(\mathcal{H}). \tag{1}$$

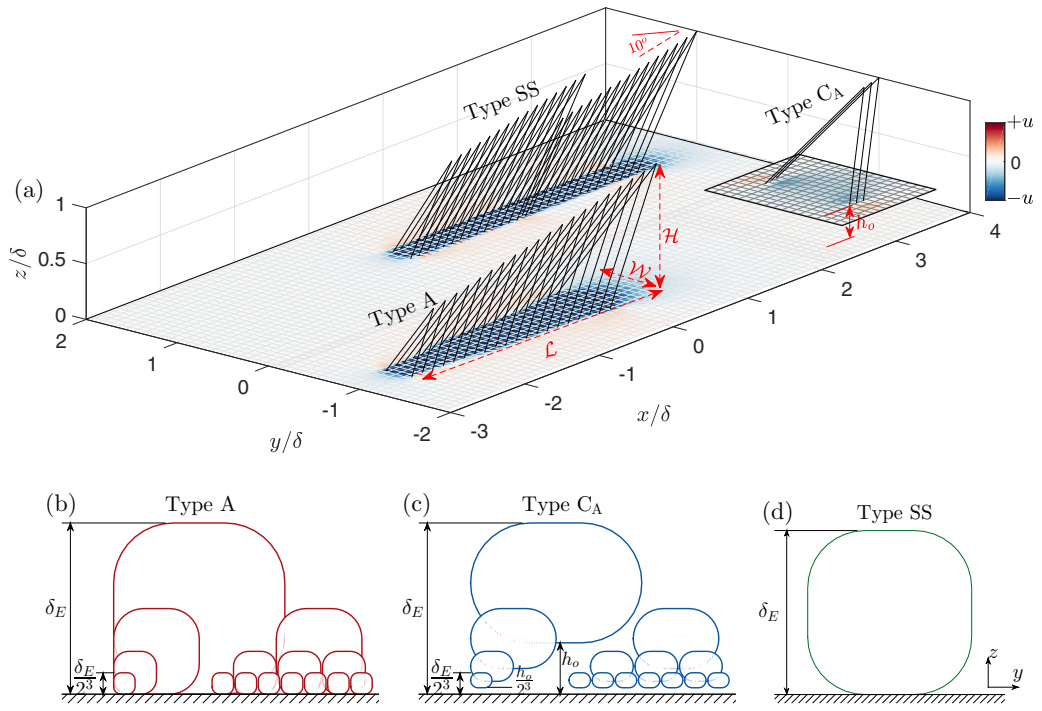

FIG. 3. (a) Geometry of Type A, Type C_A, and Type SS representative packet eddies considered in the extended model with their respective contribution to the streamwise velocity. The packet eddies are constructed by aligning geometrically scaled Λ-shaped hairpin vortices in the streamwise direction at a growth angle of 10°. $\mathcal{L}$, $\mathcal{W}$, and $\mathcal{H}$ are the characteristic length, width, and height of the eddies, respectively. [(b), (c), and (d)] Schematics showing the organization of Type A, Type C_A, and Type SS eddies, respectively. Type A (wall attached) and Type C_A (wall detached) follow a self-similar hierarchical organization, where the size and the probability density of eddies are directly and inversely proportional to z, respectively. The largest Type C_A eddy is detached from the wall by h_o. Type SS is organized as a single hierarchy with $\mathcal{H} = \delta_E$.

Here Φ_{uu} is the hierarchy spectral function, which is the power spectral density of u for a hierarchy of size $\mathcal{H}$ and averaged in the wall-parallel plane at a fixed z. $\mathcal{P}(\mathcal{H}) = 1/\mathcal{H}$ is the probability density function. Further details on computing the flow statistics from AEM can be found in Perry *et al.* [22] and Woodcock and Marusic [25].

Figure 4(a) shows the 2D spectrum of Type A eddies at $z^+ = 2.6\mathrm{Re}_\tau^{1/2}$ for $\mathrm{Re}_\tau = 26\,000$ [similarly to Fig. 1(b)]. The solid and dashed black lines represent $\lambda_y/z \sim \lambda_x/z$ scaling and $\lambda_y/z \sim (\lambda_x/z)^{1/2}$ relationship, respectively, as observed in experiments. As discussed in the introduction, Type A eddies model the large scales reasonably well. Figures 4(b) and 4(c) show the inner-flow and outer-flow scaling, respectively, of contours of constant energy [$= \max(k_x k_y \phi_{uu}/U_\tau^2)/3$] within the logarithmic region, i.e., $2.6\mathrm{Re}_\tau^{-1/2} \leqslant z/\delta \leqslant 0.15$. In the model, the height of the largest eddy, δ_E (refer to Fig. 3), is used as the characteristic outer-flow length scale. This is in place of boundary layer thickness, δ, in experiments. Representative of Townsend's attached eddies, Type A eddies follow both inner-flow and outer-flow scalings. Since the geometry of Type A eddies is selected based on experimental data, the Type A spectra have energy at $\lambda_x/z > 14$ and the spectra grows along $\lambda_x/\lambda_y \approx 7$ while moving closer to the wall. Now, considering the outer-flow scaling (when scaled in δ_E) in Fig. 4(c), the large scales collapse at $\lambda_x \approx 7\delta_E$ and $\lambda_y \approx \delta_E$, as in experiments (refer to Sec. II A).

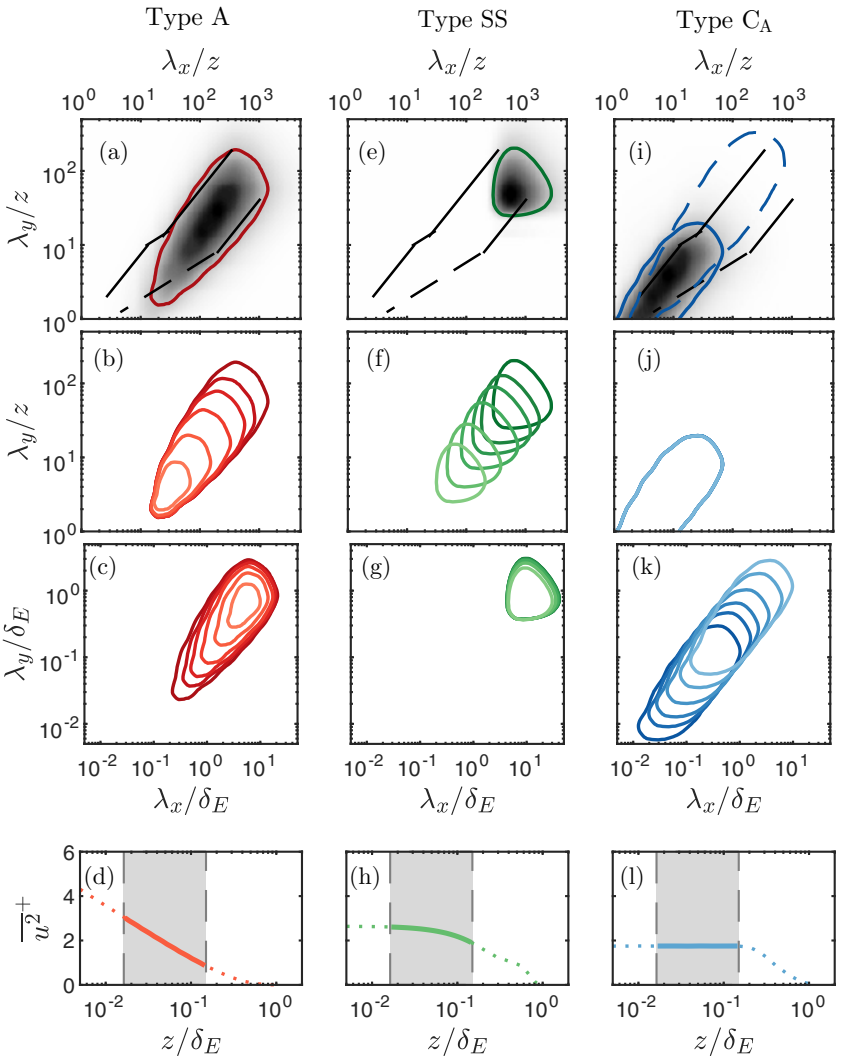

FIG. 4. [(a), (e), and (i)] Two-dimensional spectra of u, [(b), (f), and (j)] inner-flow scaling, [(c), (g), and (k)] outer-flow scaling, and [(d), (h), and (l)] profile of turbulence intensity of Type A, Type SS, and Type C_A representative eddies, respectively. Line contours represent a constant energy of $\max(k_x k_y \phi_{uu}/U_\tau^2)/3$. Dark shade to light shade is $z/\delta = 2.6\mathrm{Re}_\tau^{-1/2}$ to 0.15. The blue dashed and solid line contours in (i) are from the $h_o/\mathcal{H} = 0$ (attached) case and the $h_o/\mathcal{H} = 0.15$ case, respectively. The black solid and dashed lines in (a), (e), and (i) denote the $\lambda_y/z \sim \lambda_x/z$ scaling and $\lambda_y/z \sim (\lambda_x/z)^{1/2}$ relationship, respectively.

Figure 4(d) shows the wall normal profile of turbulence intensity ($\overline{u^2}^+$), which is obtained by integrating the 2D spectrum along both the streamwise and spanwise length scales, i.e.,

$$\overline{u^2}^+ = \int_0^\infty \int_0^\infty \frac{k_x k_y \phi_{uu}}{U_\tau^2} \, \mathrm{d}(\ln \lambda_x) \mathrm{d}(\ln \lambda_y). \tag{2}$$

Following from the attached eddy hypothesis, the turbulence intensity of Type A motions decay logarithmically with increasing wall height.

B. Type SS

Type SS eddy is representative of the wall-coherent superstructures [5], also referred to as very large scale motions [50] or the "global" mode [43] that extends deep in the wall-normal direction. Following the notion of packets aligning in the streamwise direction to form longer structures [50], the Type SS representative eddy is constructed by aligning two packets as shown in Fig. 3(a). The length ($\mathcal{L}$) of the eddy is the total length of the two smaller packets put together. The growth angle of each packet and the spacing of hairpins within the packet are consistent with the other representative eddies. $\mathcal{L}$ and $\mathcal{W}$ are chosen such that the energy contributed by Type SS motions is restricted only to the very large length scales [Fig. 4(e)]. Unlike the hierarchical structure of the Type A and Type C_A eddies, as shown in Fig. 3, the Type SS eddy is organized as a single hierarchy with the height of the eddy $\mathcal{H} \sim \delta_E$, thereby making its contribution "global" and non-self-similar with wall height [Fig. 4(f)]. Following the discussion in Sec. II A, Fig. 4(g) shows that the energy contributed by the Type SS eddy is concentrated at the fixed outer-flow scaled wavelengths of $\lambda_x/\delta_E \approx 10$ and $\lambda_y/\delta_E \approx 1$, throughout the logarithmic region. A good collapse of the constant energy contours with outer-scaling implies a roughly constant energy contribution of Type SS structures within the logarithmic region and, consequently, the profile of $\overline{u^2}^+$, as plotted in Fig. 4(h), has an almost zero slope. We note that the profile is not perfectly flat owing to the shape of the representative eddy. However, this subtle trend is found not to affect the logarithmic profile of turbulence intensity in the composite model.

C. Type C_A

Marusic and Monty [29] describe the wall-incoherent motions as Type C eddies that comprise of Kolmogorov-type fine-scale turbulence and other wall-detached motions, some of which scale self-similarly with z. In the present study, we only model the inviscid subset of Type C motions, namely Type C_A, which represent structures that are physically detached from the wall but obey a distance from the wall scaling. For simplicity, a packet eddy with similar growth angle and hairpin spacing as Type A and Type SS is considered for Type C_A as well [Fig. 3(a)]. The organization of Type C_A eddies in the boundary layer is illustrated in Fig. 3(c) with a discrete model, showing four different hierarchies. It should be noted that the organization of Type C_A eddies is very similar to that of Type A; the major difference being that the Type C_A eddies are detached from the wall. The separation from the wall of a hierarchy of eddies of size $\mathcal{H} \sim \delta_E$ is h_o, and as illustrated in Fig. 3(c), the wall-normal separation of any Type C_A eddy must be a constant fraction of its wall-normal extent. This implies that the separation from the wall of Type C_A eddies scales with z. Therefore, even when the legs of the hairpins do not extend all the way to the wall, Type C_A eddies could be regarded as "attached" in the sense of Townsend's attached eddy hypothesis since their length scales relate to the distance from the wall [29]. A similar organization was adopted for the Type B eddies of Perry and Marusic [51] and Marusic and Perry [23], in order to model the "wake-structure" in the outer layer.

The physical dimensions of the representative Type C_A eddy, which includes $\mathcal{L}$, $\mathcal{W}$, and h_o, are chosen such that the energy contribution is concentrated at the smaller scales that followed the $\lambda_y \sim \lambda_x$ relationship observed in experiments (Sec. II C). To illustrate the effect of offsetting eddies from the wall on the 2D energy spectrum, we first consider a case with zero separation from the wall, $h_o = 0$, which is typical of Type A organization. This is represented in Fig. 4(i) with the blue dashed line contour, which corresponds to a constant energy of $\max(k_x k_y \phi_{uu}/U_\tau^2)/3$. For $h_o = 0$, at each wall height z, the eddies with wall-normal extent $z \leqslant \mathcal{H} \leqslant \delta_E$ contributes to the turbulent kinetic energy. Hence the contour is observed to span a broad range of streamwise and spanwise length scales. Now if we consider a finite separation from the wall for the eddies, the 2D spectrum shrinks to smaller values of λ_x/z and λ_y/z. The filled contour in Fig. 4(i) corresponds to a separation of $h_o/\mathcal{H} = 0.15$. Due to the separation, at each wall height z, the energy spectrum has contributions from eddies with wall-normal extent $\mathcal{H} \geqslant z$ and separations $h_o \leqslant z$. Such an organization would

imply that at all wall heights below the separation of the largest eddy, i.e., at all $z < 0.15\,\delta_E$, the energy contribution is always from a fixed number of hierarchies. Consequently, when the length scales are normalized by the distance from the wall, z, the constant energy contours collapse across all wall heights within the logarithmic region [see Fig. 4(j)]. This results in an invariant distribution of $\overline{u^2}^+$ for $z < 0.15\,\delta_E$, as shown in Fig. 4(l). Further, it is observed from Fig. 4(k) that the energy of the Type C_A eddies do not scale in outer units and shift to larger length scales while moving away from the wall.

Marusic and Monty [29] reports the plausibility that self-similar but wall-incoherent energetic structures could be the detached remnants of formerly attached eddies (Type A). Although beyond the scope of the current kinematic model, an understanding of the mechanisms [4,46,47,52,53] leading to the generation of Type C_A motions is required, particularly in the context of AEM.

D. Extended AEM

The extended AEM constructed here is a composite model of Type A, Type SS, and Type C_A eddies. The 2D spectra from the AEM is hence computed as

$$k_x k_y \phi^+_{uu,\mathrm{COMP}} = \frac{(k_x k_y \phi_{uu,A} + W_{\mathrm{SS}} \times k_x k_y \phi_{uu,\mathrm{SS}} + W_{\mathrm{CA}} \times k_x k_y \phi_{uu,\mathrm{CA}})}{U^2_{\tau,\mathrm{COMP}}}, \tag{3}$$

where

$$U^2_{\tau,\mathrm{COMP}} = \max(-\overline{uw}_{\mathrm{COMP}}) \tag{4}$$

and

$$\overline{uw}_{\mathrm{COMP}} = \int\!\!\int_{-\infty}^{\infty} \Big((k_x k_y \phi_{uw,A} + W_{\mathrm{SS}} \times k_x k_y \phi_{uw,\mathrm{SS}} + W_{\mathrm{CA}} \times k_x k_y \phi_{uw,\mathrm{CA}}) \Big) \, \mathrm{d}(\ln \lambda_x)\mathrm{d}(\ln \lambda_y). \tag{5}$$

Here $k_x k_y \phi_{uu,A}$, $k_x k_y \phi_{uu,\mathrm{SS}}$, and $k_x k_y \phi_{uu,\mathrm{CA}}$ represent the 2D spectrum of u from Type A, Type SS, and Type C_A eddies, respectively. W_{SS} and W_{CA} are the relative weightings for the energy contributions from Type SS and Type C_A eddies, respectively, in relation to the energy contribution from Type A eddies. The values of W_{SS} and W_{CA} are chosen to be 0.4 and 14, respectively, in order to match the shape of the composite 2D spectrum with experiments (discussed in Sec. IV A). The composite friction velocity, $U_{\tau,\mathrm{COMP}}$ is computed by forcing the inner-normalized peak Reynolds shear stress in the logarithmic region to be unity [54], i.e., peak $-\overline{uw}^+_{\mathrm{COMP}} = \max(-\overline{uw}_{\mathrm{COMP}}/U^2_{\tau,\mathrm{COMP}}) = 1$. As represented in Eq. (5), $\overline{uw}_{\mathrm{COMP}}$ is computed by integrating the composite 2D uw spectrum across λ_x and λ_y. The same weightings (W_{SS} and W_{CA}) for the Type SS and Type C_A contributions, as in Eq. (3), are used in Eq. (5).

We note that the objective of introducing the relative weightings, W_{SS} and W_{CA}, in the composite model is not to match the magnitude of $k_x k_y \phi_{uu}/U^2_\tau$ with experimental values but to get the distribution of energy among the correct length scales, i.e., to get the correct shape of the 2D spectrum. The prescribed values for W_{SS} and W_{CA} do not vary with respect to Reynolds numbers, wall locations, or the components of velocity and therefore do not affect the scaling arguments and the conclusions drawn based on the extended model. However, we note that these weightings are specific for the current representative eddies [Fig. 3(a)] and would change with the shape of the hairpin, spacing between hairpins in a packet, strength of the vortex rods, etc. Further, the geometry of candidate eddies and their associated weightings are specified based on the 2D spectra obtained for turbulent boundary layers and hence any attempt to model the internal pipe or channel flows would have to account for the large-scale differences due to the flow geometry [32,55,56].

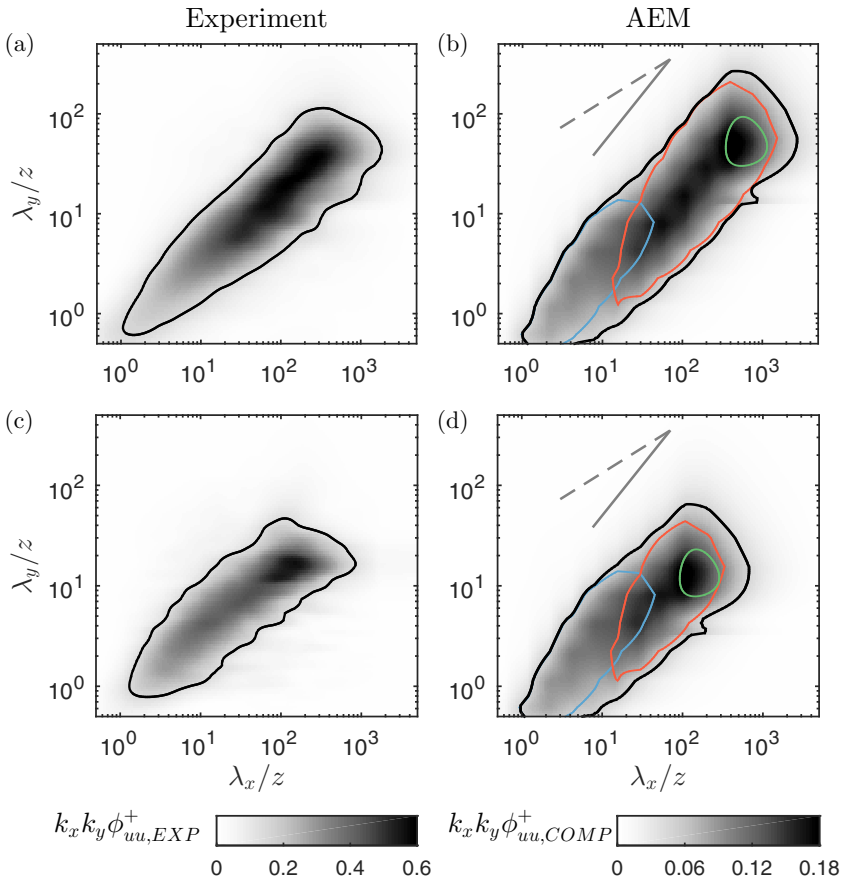

FIG. 5. Comparison of 2D spectra of u from the extended AEM with experiments at $z^+ = 2.6\mathrm{Re}_\tau^{1/2}$ for [(a) and (b)] $\mathrm{Re}_\tau \approx 26\,000$ and [(c) and (d)] $\mathrm{Re}_\tau \approx 2400$. The line contour represents $\max(k_x k_y \phi^+_{uu})/4$. In (b) and (d) black, red, green, and blue contours represent composite, Type A, Type SS, and Type $\mathrm{C_A}$ spectra, respectively, and the gray solid and dashed lines are the references for $\lambda_y/z \sim \lambda_x/z$ scaling and $\lambda_y/z \sim (\lambda_x/z)^{1/2}$ relationship, respectively.

IV. RESULTS FROM THE EXTENDED AEM

A. Spectra of u

Figures 5(a) and 5(b) show the 2D spectra of u at $\mathrm{Re}_\tau \approx 26\,000$ and $z^+ = 2.6\mathrm{Re}_\tau^{1/2}$ from the experiments and the extended model, respectively. The line contours represent $\max(k_x k_y \phi^+_{uu}/4)$. Additionally, in Fig. 5(b), the contributions of Type A, Type SS, and Type $\mathrm{C_A}$ eddies to the composite spectra is shown with red, green, and blue contours, respectively. It is observed from Figs. 5(a) and 5(b) that the composite spectra obtained with the extended AEM captures the major trends observed in the high-Re experimental 2D spectra. While the conventional AEM that comprises Type A eddies alone [red contour in Fig. 5(b)] represents only the large scales in the 2D spectra, the extended model predicts a broader range of length scales from $\mathcal{O}(z)$ to $\mathcal{O}(10\delta)$. The $\lambda_y/z \sim \lambda_x/z$ behavior observed at the smaller length scales in experimental spectra and del Álamo *et al.* [40] is now captured using Type $\mathrm{C_A}$ eddies. The shape of the 2D spectra at very large length scales is also comparable with experiments due to Type SS contributions. Interestingly, the length scales, where Type $\mathrm{C_A}$ and Type A spectra overlap, is observed to follow a near-square-root $[\lambda_y/z \sim (\lambda_x/z)^{1/2}]$ behavior. This agrees with experiments where the square-root relationship was

observed to bridge the two $\lambda_y \sim \lambda_x$ relationships observed at smaller [$\lambda_x, \lambda_y \sim \mathcal{O}(z)$] and larger [$\lambda_x, \lambda_y > \mathcal{O}(10z)$] length scales, as discussed in Sec. II.

Contrary to high-Re spectra, the square-root relationship is predominant at low Re, even at larger scales. Hence, the conventional AEM with Type A eddies alone does not predict the large scales at low Re [red line contour in Fig. 5(d)]. Since the extended AEM incorporates the low-Re characteristics with Type C_A contributions, a better prediction is observed even at low Reynolds numbers, as shown in Fig. 5(d). It is observed that at low Reynolds number ($Re_\tau \approx 2400$), the range of length scales for Type A is narrow compared to $Re_\tau \approx 26\,000$ and hence the scale separation between Type C_A and Type SS is less. Therefore, the Type A, Type C_A, and Type SS energy spectra overlap at the larger length scales, resulting in a trend similar to the $\lambda_y/z \sim (\lambda_x/z)^{1/2}$ relationship, as observed in the experimental low-Reynolds-number spectrum [Figs. 5(c) and 5(d)]. The weaker Type A contribution at low Reynolds numbers prohibits a transition of this square-root relationship to a $\lambda_y/z \sim \lambda_x/z$ trend observed at high Reynolds numbers.

1. Inner-flow scaling of 2D spectra of u

The inner-flow scaling (z scaling) of the 2D spectra of u, obtained from the extended AEM at $Re_\tau \approx 26\,000$ and computed at different wall heights, is shown in Fig. 6(b). The results are compared against the experimental spectra [Fig. 6(a)] at matched Reynolds number and wall heights. The comparison reveals a good agreement between Figs. 6(a) and 6(b) with the 2D spectra showing a good collapse at the smaller streamwise and spanwise wavelengths [$\mathcal{O}(z)$ to $\mathcal{O}(10z)$] for the wall heights considered. Figures 6(c) and 6(d) show that this collapse is a result of the perfect z scaling of the Type C_A spectra and the small-scale end of Type A spectra. The Reynolds number invariance and hence the low-Re trend at the small scales is effected by the Type C_A contribution, which follows a $\lambda_y/z \sim \lambda_x/z$ relationship. Within the region of collapse, this linear growth is observed to transition toward a square root $\lambda_y/z \sim (\lambda_x/z)^{1/2}$ behavior when there is an overlap between the Type C_A and Type A energies. Now at wavelengths larger than $(\lambda_x, \lambda_y) \sim \mathcal{O}(10z)$ in the *large-eddy region*, the spectra deviate from the scaling and trend toward the $\lambda_y/z \sim \lambda_x/z$ relationship, as observed in experiments. This transition toward a linear relationship in the *large-eddy region* is dictated by Type A energy [Fig. 6(d)] and therefore the $\lambda_y/z \sim \lambda_x/z$ scaling is more pronounced, due to the increasing contribution of Type A, as we move closer to the wall (or increasing Re_τ at $z \gg \nu/U_\tau$). We note that a peel-off from the z scaling at the very small scales is not observed in the AEM since the high-frequency Kolmogorov-type motions are not modeled.

Since 1D streamwise spectra has been a popular tool to observe self-similarity, the composite 1D streamwise spectra highlighting the contributions from Type C_A, Type A, and Type SS eddies is shown as Figs. 6(f), 6(g), and 6(h), respectively. Figures 6(f), 6(g), and 6(h) are obtained by integrating Figs. 6(c), 6(d), and 6(e), respectively, across the whole range of spanwise length scales λ_y as:

$$k_x \phi^+_{uu}(k_x) = \int_0^\infty k_x k_y \phi^+_{uu}(k_x, k_y)\, \mathrm{d}(\ln \lambda_y). \tag{6}$$

Figures 6(f), 6(g), and 6(h) are qualitatively comparable with the triple-decomposed spectra of Baars and Marusic [35] [Fig. 15(f), 15(d), and 15(b) respectively in their paper] where the decomposition technique used empirically obtained coherence-based filters. As observed by Baars and Marusic [35], the maxima of the wall-incoherent small-scale (Type C_A) energy is located at $\lambda_x \sim \mathcal{O}(10z)$. Additionally, beyond $\lambda_x \sim \mathcal{O}(10z)$, the Type A spectra is observed to ramp up with its amplitude increasing with decreasing wall height. The ramp-up of the Type A spectra at its small-scale end scales with z, which is in agreement with the empirical observation of Baars and Marusic [35]. As indicated in Figs. 6(e) and 6(h), Type SS motions do not contribute to the wall scaling of the composite spectra.

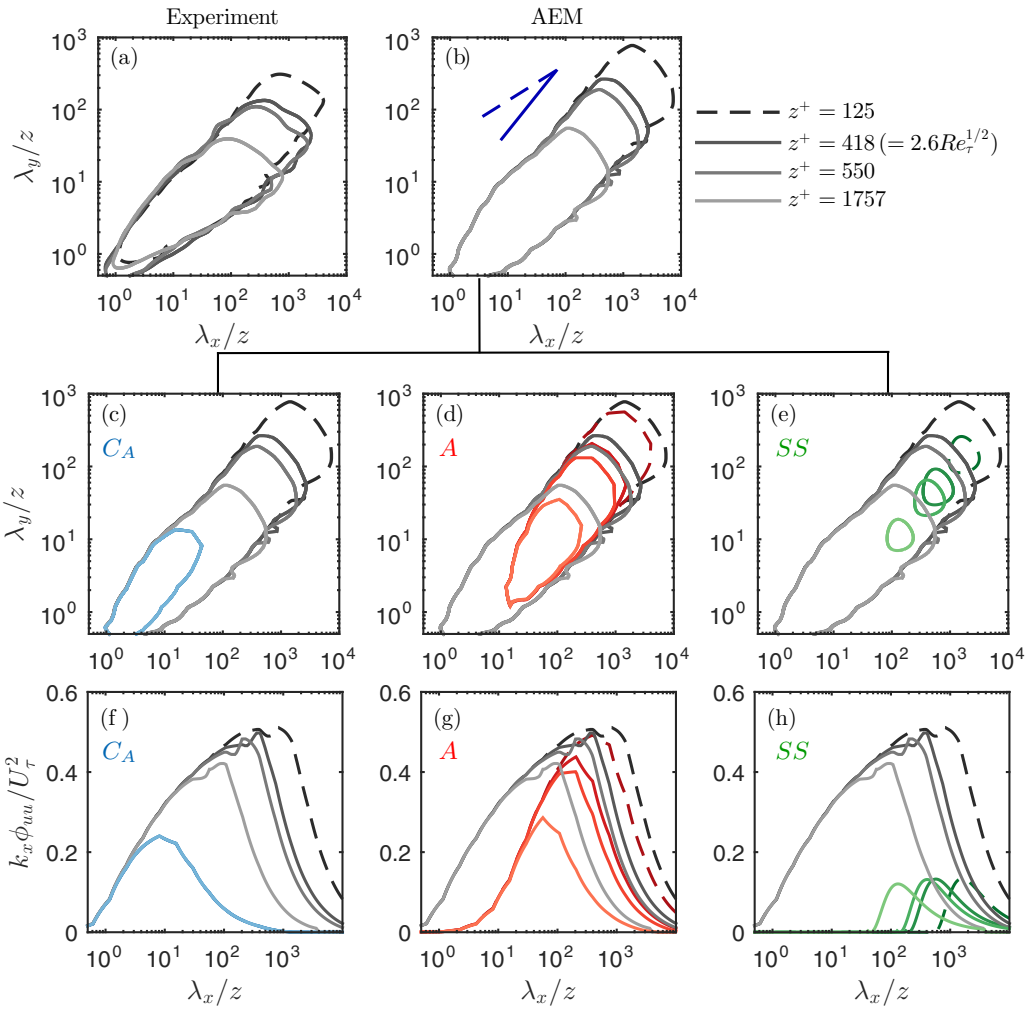

FIG. 6. Inner-flow scaling of 2D spectra of u: (a) Experiments at $\mathrm{Re}_\tau \approx 26\,000$. (b) Composite spectra from the extended AEM at $\mathrm{Re}_\tau \approx 26\,000$. [(c), (d), and (e)] Highlighting Type $\mathrm{C_A}$ (blue), Type A (red) and Type SS (green) contributions to the composite 2D spectra and [(f), (g), and (h)] highlighting Type $\mathrm{C_A}$, Type A, and Type SS contributions to the composite 1D streamwise spectra. The line contours represent a constant energy of $\max(k_x k_y \phi^+_{uu}|_{z^+=125})/4$. The blue solid and dashed lines in (b) are the references for $\lambda_y/z \sim \lambda_x/z$ scaling and $\lambda_y/z \sim (\lambda_x/z)^{1/2}$ relationship, respectively.

2. Outer-flow scaling of 2D spectra of u

The outer-flow scaling (δ scaling) of the composite 2D spectra of u, obtained from the extended AEM, at $\mathrm{Re}_\tau \approx 26\,000$ and computed at different wall heights is shown in Fig. 7(b) and are compared against experiments [Fig. 7(a)]. As observed in experimental data, the composite 2D spectra show a good collapse at scales larger than $\lambda_x \approx 7\delta_E$ and $\lambda_y \approx \delta_E$ for all wall heights considered. As observed in Figs. 7(d) and 7(e), this collapse is due to the δ-scaled contributions from the Type SS eddies and the large-scale end of Type A. Now as observed in experiments, for $\lambda_x < 7\delta_E$ in the *large-eddy region*, the constant energy contour deviates from a perfect δ scaling while following the relationship of $\lambda_y/\delta \sim (\lambda_x/\delta)^m$. The value of m is observed to transition from

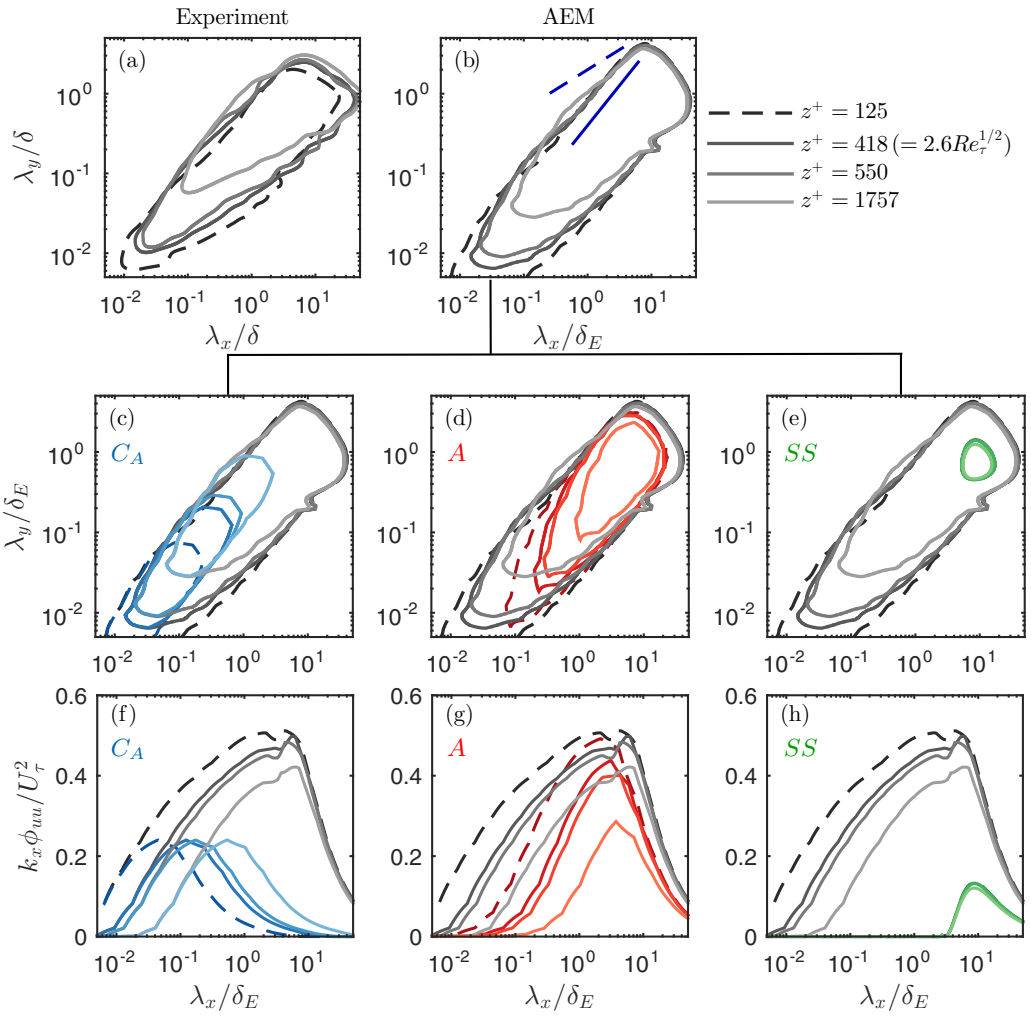

FIG. 7. Outer-flow scaling of 2D spectra of u when the wavelengths are normalized by the boundary layer thickness δ (in experiments) or the height of the largest eddy δ_E (in AEM). Details of the plots are the same as in Fig. 6.

0.5 to 1 [represented by dashed and solid blue lines respectively in Fig. 7(b)] as we move closer to the wall. From Figs. 7(c) to 7(e), we see that this trend toward $m = 1$ with decreasing z is due to the increased Type A contribution and thus the increased scale separation between Type SS and Type C_A energies.

The δ-scaled composite 1D streamwise spectra highlighting the contributions from Type C_A, Type A, and Type SS eddies are shown as Figs. 7(f), 7(g), and 7(h), respectively. Figures 7(f), 7(g), and 7(h) are comparable with the triple-decomposed spectra of Baars and Marusic [35] [Fig. 15(e), 15(c), and 15(a), respectively, in their paper]. As observed by Baars and Marusic [35], the maxima of the wall-coherent very large scale (Type SS) energy is located at $\lambda_x \sim \mathcal{O}(10\delta_E)$. The roll-off at the large-scale end of Type A spectra is observed to follow δ scaling in agreement with the empirical observation of Baars and Marusic [35] for $2.6\mathrm{Re}_\tau^{1/2} \leqslant z^+ \leqslant 0.15\delta^+$. As indicated in Figs. 7(c) and 7(f), Type C_A motions do not contribute to the outer-flow scaling of the composite spectra.

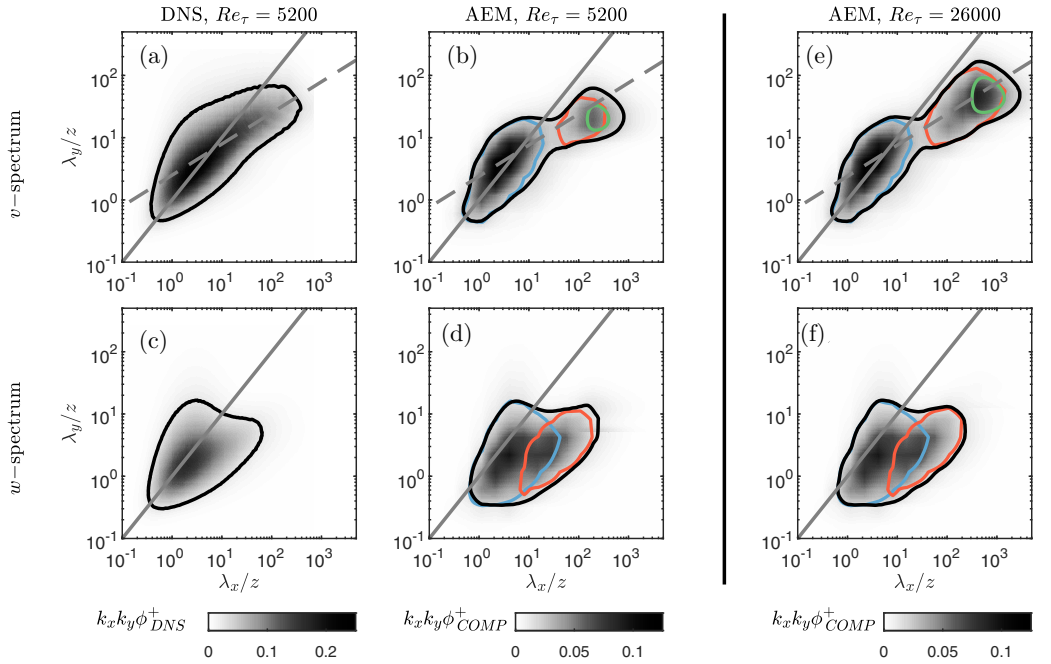

FIG. 8. [(a)–(d)] Comparison of the extended AEM with DNS of Lee and Moser [57] at $\mathrm{Re}_\tau = 5200$ and $z^+ = 2.6\mathrm{Re}_\tau^{1/2}$; [(a) and (b)] spectra of spanwise velocity (v); and [(c) and (d)] spectra of wall-normal velocity (w). [(e) and (f)] Spectra of v and w, respectively, as predicted by the extended AEM for $\mathrm{Re}_\tau = 26\,000$. The line contours in all panels represent a constant energy of $\max(k_x k_y \phi^+)/6$. In (b), (d), (e), and (f) black, red, green, and blue contours represent composite, Type A, Type SS, and Type $\mathrm{C_A}$ spectra, respectively. The gray solid and dashed lines denote $\lambda_y/z = \lambda_x/z$ and $\lambda_y/z \sim (\lambda_x/z)^{1/2}$, respectively.

B. Spectra of v and w

In the present study, the extension to the AEM was driven by scaling of the 2D spectra of the streamwise velocity u alone, since only u data are available at high Reynolds number. We can now assess whether the extended AEM also provides better predictions for the spectra of the spanwise (v) and the wall-normal (w) velocity components. The composite 2D spectra of v and w are computed from the model similar to the computation of the spectra of u [Eq. (3)] with the values of W_{CA} and W_{SS} remaining the same. The results from the model are compared with the DNS of Lee and Moser [57] at $\mathrm{Re}_\tau = 5200$ in Figs. 8(a)–8(d). We chose this dataset as it is the highest Re data available for the 2D spectra of v and w. As in Figs. 8(a)–8(d), spectra of v and w from the extended AEM show good agreement with DNS. It is seen from the DNS data that the dominant streamwise and spanwise modes in both v and w spectra are $\mathcal{O}(z)$. These energetic modes are represented in the model with the major contribution from Type $\mathrm{C_A}$ eddies for the $\mathrm{Re}_\tau = 5200$ case. As shown in Figs. 8(b) and 8(d), a model with Type A eddies alone (red line contours) represent the dominant modes at much larger length scales in the v and w spectra (as also observed by Baidya *et al.* [27]) and misses a large contribution to the overall energy. It is observed that the energy not represented by Type A eddies, or the conventional AEM, is more significant for the v and w spectra in comparison to the spectra of u.

At low Reynolds number ($\mathrm{Re}_\tau = 2000$), Jiménez and Hoyas [58] reported from their DNS of a channel flow that the energetic ridge of the 2D spectra of v and w follow a $\lambda_y/z = \lambda_x/z$ relationship in the log region. However, from the data at higher Reynolds numbers ($\mathrm{Re}_\tau = 5200$,

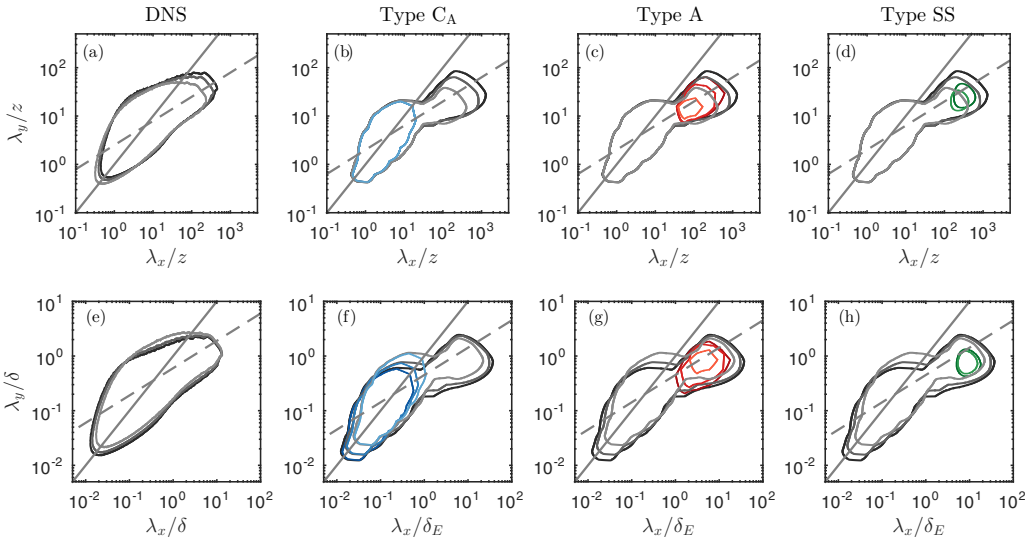

FIG. 9. Inner-flow scaling of 2D spectra of v from (a) the DNS of Lee and Moser [57] and [(b), (c), and (d)] extended AEM highlighting the contributions from Type C_A (blue), Type A (red), and Type SS (green) to the v spectra, respectively, at $z^+ = 150,\ 2.6\mathrm{Re}_\tau^{1/2}$, and $3.9\mathrm{Re}_\tau^{1/2}$ (dark to light shade, respectively). [(e)–(h)] Similar plots in outer-flow scaling. The line contours represent a constant energy of $\max(k_x k_y \phi^+_{vv}|_{z^+=150})/6$. The gray solid and dashed lines denote $\lambda_y = \lambda_x$ and $\lambda_y \sim (\lambda_x)^{1/2}$, respectively.

DNS), we see that in the v spectra, above scales $\mathcal{O}(10z)$, the $\lambda_y/z = \lambda_x/z$ relationship transitions to a square-root relationship of $\lambda_y/z \sim (\lambda_x/z)^{1/2}$, similarly to the trend observed in the 2D spectra of u. This trend is expected as u and v spectra follow similar scaling laws [22]. To understand this better, the inner-flow and outer-flow scaling of the composite 2D spectra of v is plotted in Fig. 9 highlighting the contributions of Type C_A, Type A, and Type SS eddies. The predominant low-Re trend of $\lambda_y/z = \lambda_x/z$ is due to the Type C_A contribution that scales with z. As observed for the u spectra, the transition to a square-root relation appears to be at scales $\mathcal{O}(10z)$ where the Type C_A and the Type A energies overlap. At scales larger than $\mathcal{O}(10z)$, the shape of the 2D spectra is dictated by Type A energy which seem to gradually transition toward a $\lambda_y/z \sim \lambda_x/z$ relationship. However, the current Reynolds number ($\mathrm{Re}_\tau = 5200$) is not high enough for this linear trend to be conspicuous. Figures 8(e) and 8(f) show the predictions of v and w spectra from the extended AEM at $\mathrm{Re}_\tau \approx 26\,000$. Similarly to the *large-eddy region* in the spectra of u, the large scales [$>\mathcal{O}(10z)$] in a constant energy region of the v spectrum appear to begin to follow the $\lambda_y/z \sim \lambda_x/z$ scaling, indicating self-similarity. A validation of this self-similar trend requires the measurement of the 2D v spectra at high Reynolds numbers.

Unlike the u and v components, at a particular wall height z, only those eddies with heights $\mathcal{H} \sim z$ contribute to w spectra. Hence, as shown in Fig. 10, the w spectra follows a perfect inner-flow scaling [22,27]. Since Type SS eddies have heights $\mathcal{H} \sim \delta$, they do not contribute to the w spectra in the log region [Figs. 10(d) and 10(h)].

While the current model, which is developed based on the scaling of the u spectra, captures the key scaling arguments of the v and the w spectra, we note that further modifications are required to better model the 2D spectra of all components of velocity. For example, tuning the shape of the hairpins could possibly resolve the bimodal nature of the v spectra. However, such refinements would require 2D spectra of v and w at high Reynolds numbers.

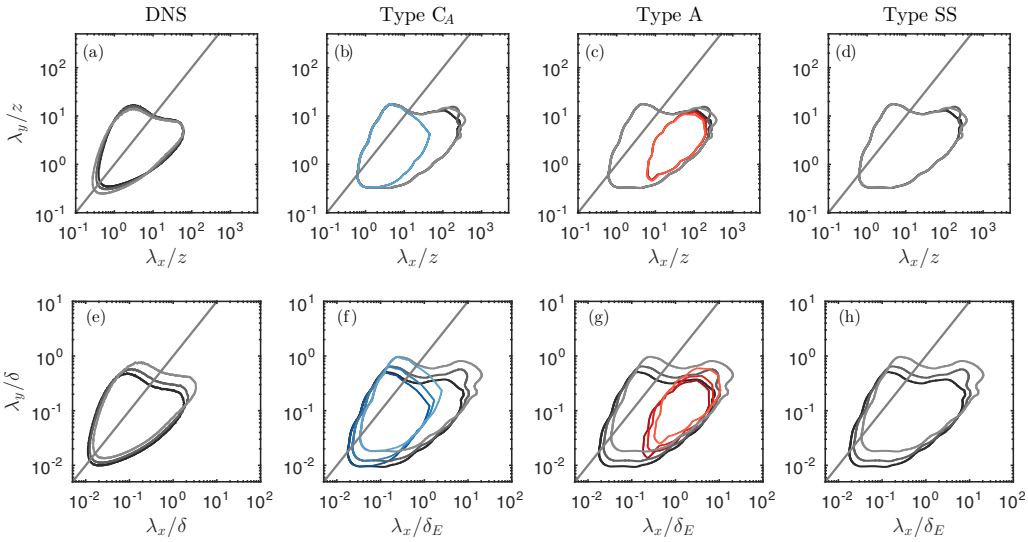

FIG. 10. Inner-flow scaling of 2D spectra of w from (a) the DNS of Lee and Moser [57] and [(b), (c), (d)] extended AEM highlighting the contributions from Type C_A (blue), Type A (red), and Type SS (green) to the w spectra, respectively, at $z^+ = 150$, $2.6\mathrm{Re}_\tau^{1/2}$, and $3.9\mathrm{Re}_\tau^{1/2}$ (dark to light shade respectively). [(e)–(h)] Similar plots in outer-flow scaling. The line contours represent a constant energy of $\max(k_x k_y \phi^+_{ww}|_{z^+=150})/6$. The gray solid line denotes $\lambda_y = \lambda_x$.

V. DISCUSSION ON SPECTRAL SELF-SIMILARITY BASED ON THE EXTENDED AEM

As discussed in Sec. II, the *large-eddy region* of the 2D spectra of u follows the relationship $\lambda_y/z \sim (\lambda_x/z)^m$, where the power-law coefficient "m" denotes the slope of the *large-eddy region*. Since 1D spectrum is simply the line integral of the 2D spectrum, the large-scale plateau A_{1x} in the 1D streamwise spectrum is the line integral of the *large-eddy region* across the range of λ_y. Similarly, A_{1y} in the 1D spanwise spectrum is the line integral of the *large-eddy region* across the range of λ_x. Based on a simplified model of the 2D spectrum, Chandran *et al.* [31] reported that the ratio A_{1x}/A_{1y} is equivalent to the slope of the *large-eddy region*, m. Further, based on experimental data, they observed the value of m $(= A_{1x}/A_{1y})$ to monotonically increase with Reynolds number toward 1, with $m = 1$ indicating self-similarity. Here, using the extended AEM, we discuss a kinematic perspective on this empirically observed trend of m with Re_τ.

Figure 11(a) shows the plot of m vs. Re_τ at $z^+ \approx 150$ from both experiments and the extended AEM, and the red dashed line indicates self-similarity. The results from the extended AEM follow the empirically observed Reynolds number trend reasonably well. We note that the values are slightly overpredicted at low Reynolds numbers while matching well with experiments for $\mathrm{Re}_\tau \gtrsim 10^4$. Agreeing with the empirical fit, the value of m obtained from the model is observed to approach unity at $\mathrm{Re}_\tau \approx 60\,000$. Here it is to be noted that a model comprising of Type A eddies alone would always predict $m = 1$ irrespective of Reynolds number (red dashed line).

In order to understand the Reynolds number trend of m, we analyze the 2D spectrum with the associated 1D streamwise and spanwise spectra at $\mathrm{Re}_\tau = 2400$ ($m \approx 0.5$) and $\mathrm{Re}_\tau = 60\,000$ ($m = 1$), obtained from the extended AEM, shown in Figs. 11(b) and 11(c), respectively. The contributions of Type A, Type C_A, and Type SS eddies are highlighted and color coded in the figure. The plateaus in the streamwise and spanwise spectra, A_{1x} and A_{1y}, are also highlighted. At $\mathrm{Re}_\tau = 2400$ [Fig. 11(b)], there is less scale separation between the largest (Type SS) and the

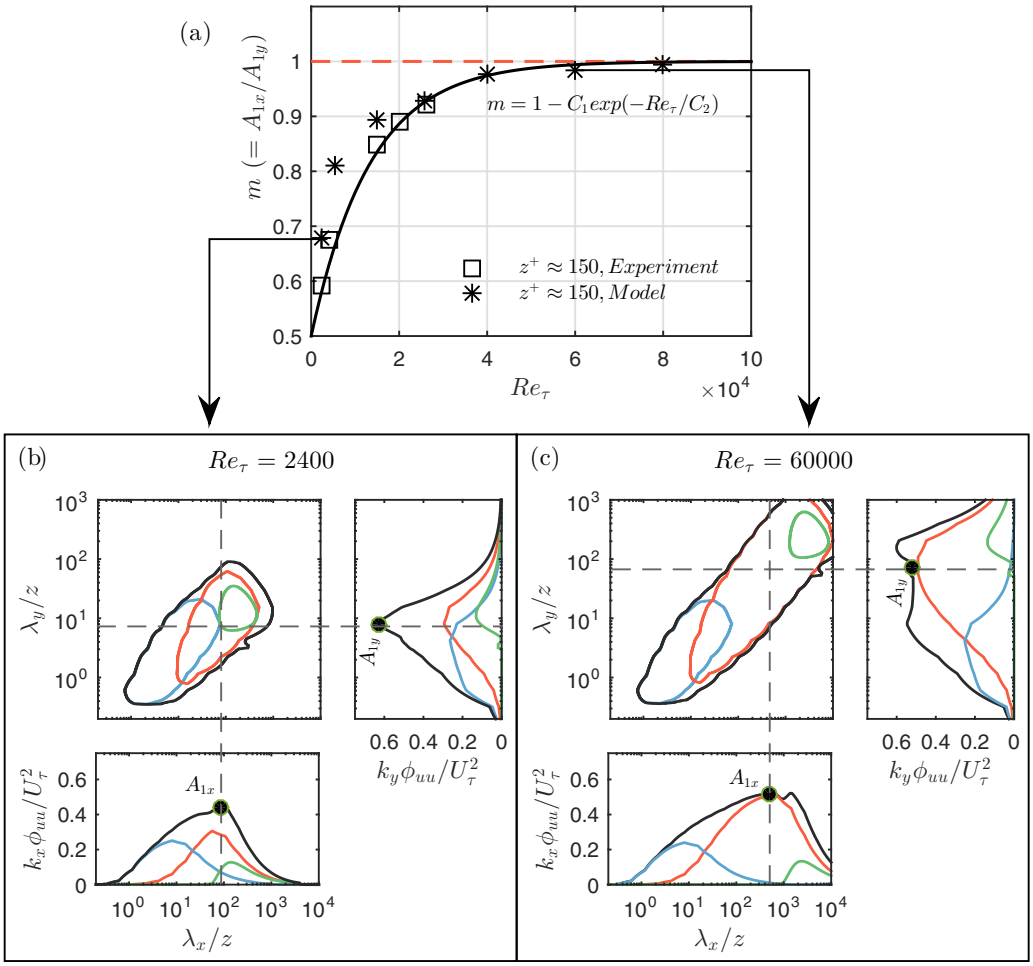

FIG. 11. (a) Variation of m versus Re_τ at $z^+ \approx 150$ from experiments and the extended AEM. The solid black curve is the empirical fit of the form $m = 1 - C_1 \exp(-\mathrm{Re}_\tau/C_2)$ from Chandran *et al.* [31], where $C_1 = 0.5$ and the value of C_2 is simply fitted to the data. [(b) and (c)] Two-dimensional spectrum and the associated 1D spectra at $\mathrm{Re}_\tau = 2400$ and $\mathrm{Re}_\tau = 60\,000$, respectively, from the extended AEM. The energy contribution of Type $\mathrm{C_A}$ (blue), Type A (red), and Type SS (green) motions are plotted in (b) and (c).

smallest (Type $\mathrm{C_A}$) energetic motions, which result in an overlap of the energy contributions from Type $\mathrm{C_A}$, Type A, and Type SS eddies for $\lambda_x > \mathcal{O}(10z)$ and $\lambda_y > \mathcal{O}(z)$. As discussed in Sec. IV A, the $\lambda_y/z \sim (\lambda_x/z)^{1/2}$ relationship ($m = 0.5$) at such length scales is observed to be a result of the overlap of subcomponent energies. The 1D streamwise and spanwise spectra are obtained by integrating the 2D spectrum as given in Eq. (6). Therefore, the plateaus in the 1D streamwise and spanwise spectra, A_{1x} and A_{1y}, respectively, are obtained by integrating the 2D spectrum along the vertical and the horizontal dashed lines in Fig. 11(b), respectively. At $\mathrm{Re}_\tau = 2400$, A_{1x} and A_{1y} have contributions from all three spectral subcomponents: Type $\mathrm{C_A}$, Type A, and Type SS. Since Type $\mathrm{C_A}$ energy diminishes beyond $[\lambda_x/z, \lambda_y/z] \sim 10$, its contribution to A_{1x} at $\lambda_x/z \sim 100$ is from its roll-of and therefore is relatively low. However, for the plateau in the spanwise spectra A_{1y}, which is at $\lambda_y/z \sim 10$, the contribution of Type $\mathrm{C_A}$ is high and in proportion to that of Type A. Since Type A and Type SS contribute similarly to A_{1x} and A_{1y}, the increased contribution from Type $\mathrm{C_A}$ to A_{1y} results in $A_{1y} > A_{1x}$ and, therefore, $m < 1$.

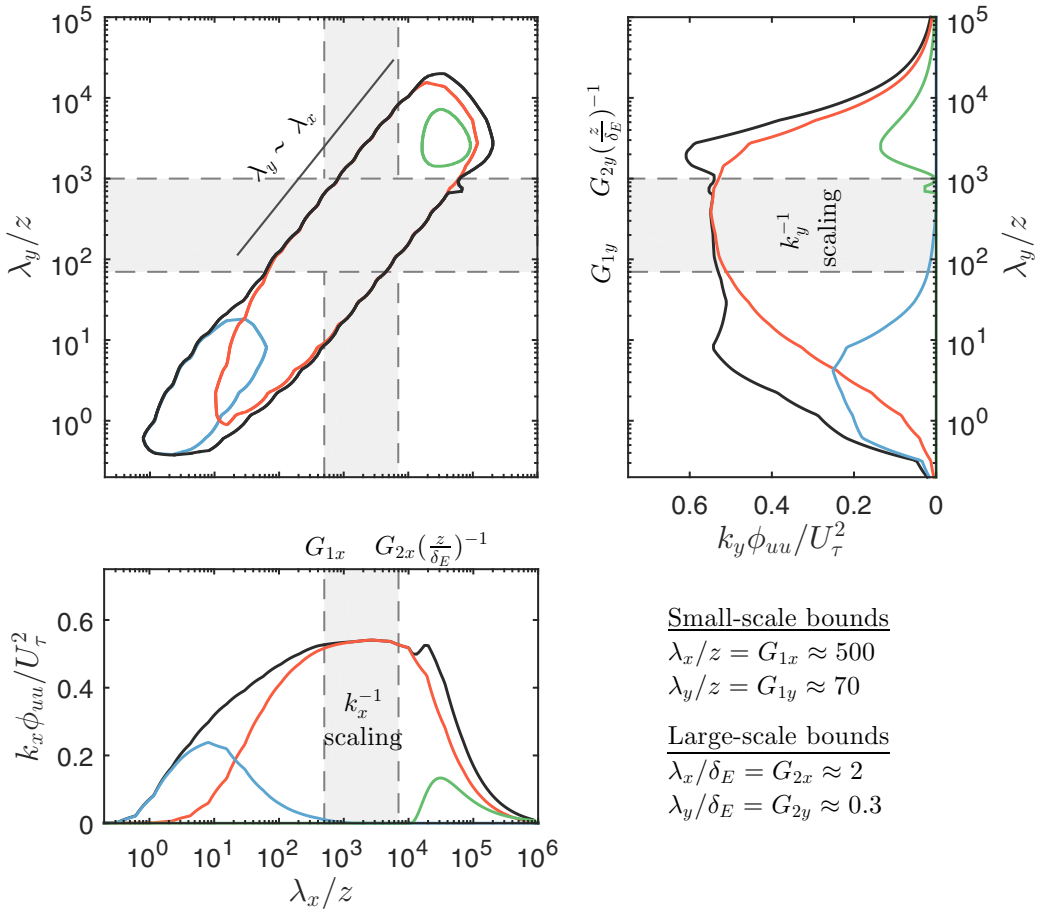

FIG. 12. Spectra of u at $z/\delta_E \sim 10^{-4}$ for an asymptotic high Reynolds number such that $z \gg \nu/U_\tau$. A decade of k^{-1} plateau in both streamwise and spanwise spectra is highlighted. The small-scale and large-scale bounds of the k^{-1} region is indicated in the plots. The energy contribution of Type C_A (blue), Type A (red), and Type SS (green) motions are highlighted.

The scale separation between the largest and the smallest scales increases with Reynolds number. Referring back to Fig. 4, Type C_A and the small-scale end of Type A follow inner-flow scaling while Type SS and the large-scale end of Type A follow outer scaling. Therefore, with increasing Reynolds number (or decreasing z/δ), Type SS spectra and the large-scale end of Type A spectra shift to larger λ_x/z and λ_y/z. As seen from Fig. 11(c), at $\mathrm{Re}_\tau = 60\,000$, Type C_A and Type SS spectra are completely separated from each other at the wavelengths corresponding to the locations of A_{1x} and A_{1y} which are $\lambda_x/z \approx 500$ and $\lambda_y/z \approx 70$, respectively. As a consequence, at this Reynolds number, A_{1x} and A_{1y} have energy contributions only from the wall-coherent self-similar Type A motions (spectra in red). Hence, from Fig. 11(c), $\lambda_x/z \approx 500$ and $\lambda_y/z \approx 70$ represent the length scales at which a true k^{-1} scaling commences in a 1D streamwise and 1D spanwise spectra, respectively. Even though a true k^{-1} scaling kicks in at $\mathrm{Re}_\tau \approx 60\,000$, a decade of k^{-1} scaling may be revealed only at even higher Reynolds numbers.

The prediction from the model at an extreme Re_τ is shown in Fig. 12 where a decade of k^{-1} scaling is evident in both streamwise and spanwise spectra. The small-scale bound of the k^{-1} region corresponds to the small-wavelength end of Type A energy that is no longer overlapped by Type

C_A contribution, i.e., where the "large-scale roll-off" from Type C_A energy ends. Since this roll-off scales with z, the k^{-1} region begins at fixed inner-scaled wavelengths, G_{1x} and G_{1y}, respectively, in the 1D streamwise and spanwise spectra. Based on the results from the extended AEM, these bounds are estimated to be $\lambda_x/z = G_{1x} \approx 500$ and $\lambda_y/z = G_{1y} \approx 70$, respectively. The limit in the streamwise spectra agrees with Baars and Marusic [35], who estimated $G_{1x} \approx 385$. Similarly, the large-scale bound of the k^{-1} region corresponds to the large-wavelength end of Type A energy that is no longer overlapped by Type SS contribution, i.e., where the "small-scale roll-off" from Type SS energy ends. Since this roll-off scales with δ_E, the k^{-1} region at the large scales would be bounded by fixed outer-scaled wavelengths, G_{2x} and G_{2y}, respectively, in the 1D streamwise and spanwise spectra. From Fig. 12, these bounds are estimated to be $\lambda_x/\delta_E = G_{2x} \approx 2$ and $\lambda_y/\delta_E = G_{2y} \approx 0.3$, respectively. Therefore, a decade of k_x^{-1} scaling would require $G_{2x}(z/\delta_E)^{-1}/G_{1x} \sim 10$, and a decade of k_y^{-1} scaling would require $G_{2y}(z/\delta_E)^{-1}/G_{1y} \sim 10$, or in both cases, $z/\delta_E \sim 10^{-4}$ (Fig. 12). Considering $z^+ = 2.6\mathrm{Re}_\tau^{1/2}$ in the logarithmic region, $z/\delta_E \sim 10^{-4}$ would correspond to an extreme $\mathrm{Re}_\tau \sim 10^8$. However, recent high-Reynolds-number studies [31,35,36,59] suggest self-similar scales of motion to be evident even at $z^+ < 2.6\mathrm{Re}_\tau^{1/2}$ when sufficiently far from the wall ($z \gg \nu/U_\tau$). In this context, we note that an equivalent scale separation could be achieved at $\mathrm{Re}_\tau \sim 10^6$ at $z^+ \simeq 100$ ($<2.6\mathrm{Re}_\tau^{1/2}$).

We note that the conclusions from the current model are based on a perfect outer-flow scaling of Type SS energy. The work of Baars and Marusic [35] reports very large scale energy contributions to have a subtle trend with Reynolds number. The authors, however, report the trend to be weaker than previous observations [5,56,60]. Even though the trend appears to be less significant within the log region $2.6\mathrm{Re}_\tau^{1/2} \leqslant z^+ \leqslant 0.15\mathrm{Re}_\tau$, the asymptotic predictions would benefit clarity on the outer-flow scaling arguments of very large scale motions.

VI. SUMMARY AND CONCLUSIONS

The AEM comprising only self-similar wall-attached eddies (Type A) is observed to represent the dominant large scales in the logarithmic region only at high Reynolds numbers. However, when compared to experimental data, the energy left unresolved by these Type A eddies is found to be significant enough to dictate the trends of the 2D spectra, even at Reynolds numbers as high as $\mathrm{Re}_\tau = 26\,000$. Therefore, an extension to the AEM is proposed by incorporating into the model two additional types of structures that are major contributors to the turbulent kinetic energy in the logarithmic region: (i) Type C_A eddies, representative of the wall-incoherent, small-scale structures that follow a self-similar distance from the wall scaling and (ii) Type SS eddies, representative of the wall-coherent, very large scale (superstructure-like) motions or the global modes. The geometry of these representative eddies and their organization within the boundary layer are identified based on the experimentally observed inner-flow (z scaling) and outer-flow scaling (δ scaling) of the 2D energy spectra of u.

When considering the energy spectra of u, v, and w that is obtained from the extended AEM, in addition to the energy contribution from Type A eddies, there is the z-scaled energy contribution from Type C_A eddies at $[\lambda_x \sim z, \lambda_y \sim z]$ and the δ-scaled energy contribution from Type SS eddies at $[\lambda_x \sim 10\,\delta, \lambda_y \sim \delta]$. Consequently, the model captured the experimentally observed trends of the 2D energy spectra of all three velocity components reasonably well across a greater range of energetic scales from $\mathcal{O}(z)$ to $\mathcal{O}(10\,\delta)$. The model also captured the empirically observed shift in the trend of the energetic large scales in the 2D spectra of u from a $\lambda_y/z \sim (\lambda_x/z)^{1/2}$ relationship at low-Reynolds numbers toward the self-similar $\lambda_y \sim \lambda_x$ scaling at high-Reynolds numbers. A discussion on this Reynolds number trend is presented for the spectra of u, based on which self-similarity would be evident with a $\lambda_y \sim \lambda_x$ scaling for a region of constant energy in the 2D spectrum, and the associated k^{-1} scaling in the 1D streamwise and spanwise spectrum, only at $\mathrm{Re}_\tau \gtrsim 60\,000$, when a complete scale separation between the δ-scaled Type SS and the z-scaled Type C_A eddies is predicted to exist.

ACKNOWLEDGMENTS

The authors gratefully acknowledge the financial support of this research from the Australian Research Council. The authors thank Myoungkyu Lee and Robert Moser for providing the 2D spectra from turbulent channel DNS at $\mathrm{Re}_\tau = 5200$ and Woutijn Baars, Rio Baidya, Charitha de Silva, and Rahul Deshpande for helpful discussions and feedback on the manuscript.

[1] I. Marusic, R. Mathis, and N. Hutchins, High Reynolds number effects in wall turbulence, Int. J. Heat Fluid Flow **31**, 418 (2010).
[2] J. Jiménez, Cascades in wall-bounded turbulence, Annu. Rev. Fluid Mech. **44**, 27 (2012).
[3] S. K. Robinson, Coherent motions in the turbulent boundary layer, Annu. Rev. Fluid Mech. **23**, 601 (1991).
[4] R. J. Adrian, Hairpin vortex organization in wall turbulence, Phys. Fluids **19**, 041301 (2007).
[5] N. Hutchins and I. Marusic, Evidence of very long meandering features in the logarithmic region of turbulent boundary layers, J. Fluid Mech. **579**, 1 (2007).
[6] A. J. Smits, B. J. McKeon, and I. Marusic, High-Reynolds number wall turbulence, Annu. Rev. Fluid Mech. **43**, 353 (2011).
[7] A. Lozano-Durán and J. Jiménez, Time-resolved evolution of coherent structures in turbulent channels: characterization of eddies and cascades, J. Fluid Mech. **759**, 432 (2014).
[8] J. Jiménez, Coherent structures in wall-bounded turbulence, J. Fluid Mech. **842**, P1 (2018).
[9] A. A. Townsend, *The Structure of Turbulent Shear Flow*, 2nd ed. (Cambridge University Press, Cambridge, UK, 1976).
[10] J. C. Vassilicos, J.-P. Laval, J.-M. Foucaut, and M. Stanislas, The streamwise turbulence intensity in the intermediate layer of turbulent pipe flow, J. Fluid Mech. **774**, 324 (2015).
[11] Y. Hwang, Statistical structure of self-sustaining attached eddies in turbulent channel flow, J. Fluid Mech. **767**, 254 (2015).
[12] X. I. A. Yang, R. Baidya, P. Johnson, I. Marusic, and C. Meneveau, Structure function tensor scaling in the logarithmic region derived from the attached eddy model of wall-bounded turbulent flows, Phys. Rev. Fluids **2**, 064602 (2017).
[13] L. Agostini and M. Leschziner, Spectral analysis of near-wall turbulence in channel flow at $\mathrm{Re}_\tau = 4200$ with emphasis on the attached-eddy hypothesis, Phys. Rev. Fluids **2**, 014603 (2017).
[14] H. Mouri, Two-point correlation in wall turbulence according to the attached-eddy hypothesis, J. Fluid Mech. **821**, 343 (2017).
[15] J. Hwang and H. J. Sung, Wall-attached structures of velocity fluctuations in a turbulent boundary layer, J. Fluid Mech. **856**, 958 (2018).
[16] M. Cho, Y. Hwang, and H. Choi, Scale interactions and spectral energy transfer in turbulent channel flow, J. Fluid Mech. **854**, 474 (2018).
[17] A. Lozano-Durán and H. J. Bae, Characteristic scales of Townsend's wall-attached eddies, J. Fluid Mech. **868**, 698 (2019).
[18] B. J. McKeon, Self-similar hierarchies and attached eddies, Phys. Rev. Fluids **4**, 082601(R) (2019).
[19] M. Yoon, J. Hwang, J. Yang, and H. J. Sung, Wall-attached structures of streamwise velocity fluctuations in an adverse-pressure-gradient turbulent boundary layer, J. Fluid Mech. **885**, A12 (2020).
[20] Y. Hwang and B. Eckhardt, Attached eddy model revisited using a minimal quasi-linear approximation, J. Fluid Mech. **894**, A23 (2020).
[21] A. E. Perry and M. S. Chong, On the mechanism of wall turbulence, J. Fluid Mech. **119**, 173 (1982).
[22] A. E. Perry, S. Henbest, and M. S. Chong, A theoretical and experimental study of wall turbulence, J. Fluid Mech. **165**, 163 (1986).
[23] I. Marusic and A. E. Perry, A wall-wake model for the turbulence structure of boundary layers. Part 2. Further experimental support, J. Fluid Mech. **298**, 389 (1995).
[24] I. Marusic, On the role of large-scale structures in wall turbulence, Phys. Fluids **13**, 735 (2001).

[25] J. D. Woodcock and I. Marusic, The statistical behavior of attached eddies, Phys. Fluids **27**, 015104 (2015).
[26] C. M. de Silva, J. D. Woodcock, N. Hutchins, and I. Marusic, Influence of spatial exclusion on the statistical behavior of attached eddies, Phys. Rev. Fluid **1**, 022401 (2016).
[27] R. Baidya, J. Philip, N. Hutchins, J. P. Monty, and I. Marusic, Distance-from-the-wall scaling of turbulent motions in wall-bounded flows, Phys. Fluids **29**, 020712 (2017).
[28] F. Eich, C. M. de Silva, I. Marusic, and C. J. Kähler, Towards an improved spatial representation of a boundary layer from the attached eddy model, Phys. Rev. Fluids **5**, 034601 (2020).
[29] I. Marusic and J. P. Monty, Attached eddy model of wall turbulence, Annu. Rev. Fluid Mech. **51**, 49 (2019).
[30] W. J. Baars, N. Hutchins, and I. Marusic, Self-similarity of wall-attached turbulence in boundary layers, J. Fluid Mech. **823**, R2 (2017).
[31] D. Chandran, R. Baidya, J. P. Monty, and I. Marusic, Two-dimensional energy spectra in high Reynolds number turbulent boundary layers, J. Fluid Mech. **826**, R1 (2017).
[32] R. Baidya, W. J. Baars, S. Zimmerman, M. Samie, R. J. Hearst, E. Dogan, L. Mascotelli, X. Zheng, G. Bellani, A. Talamelli *et al.*, Simultaneous skin friction and velocity measurements in high Reynolds number pipe and boundary layer flows, J. Fluid Mech. **871**, 377 (2019).
[33] J. Klewicki, P. Fife, and T. Wei, On the logarithmic mean profile, J. Fluid Mech. **638**, 73 (2009).
[34] R. Deshpande, D. Chandran, J. P. Monty, and I. Marusic, Two-dimensional cross-spectrum of the streamwise velocity in turbulent boundary layers, J. Fluid Mech. **890**, R2 (2020).
[35] W. J. Baars and I. Marusic, Data-driven decomposition of the streamwise turbulence kinetic energy in boundary layers. Part 1. Energy spectra, J. Fluid Mech. **882**, A25 (2020).
[36] W. J. Baars and I. Marusic, Data-driven decomposition of the streamwise turbulence kinetic energy in boundary layers. Part 2. Integrated energy and A_1, J. Fluid Mech. **882**, A26 (2020).
[37] I. Marusic, J. P. Monty, M. Hultmark, and A. J. Smits, On the logarithmic region in wall turbulence, J. Fluid Mech. **716**, R3 (2013).
[38] J. P. Monty, Z. Harun, and I. Marusic, A parametric study of adverse pressure gradient turbulent boundary layers, Int. J. Heat Fluid Flow **32**, 575 (2011).
[39] W. J. Baars, D. T. Squire, K. M. Talluru, M. R. Abbassi, N. Hutchins, and I. Marusic, Wall-drag measurements of smooth-and rough-wall turbulent boundary layers using a floating element, Exp. Fluids **57**, 90 (2016).
[40] J. C. del Álamo, J. Jiménez, P. Zandonade, and R. D. Moser, Scaling of the energy spectra of turbulent channels, J. Fluid Mech. **500**, 135 (2004).
[41] K. A. Chauhan, P. A. Monkewitz, and H. M. Nagib, Criteria for assessing experiments in zero pressure gradient boundary layers, Fluid Dyn. Res. **41**, 021404 (2009).
[42] C. D. Tomkins and R. J. Adrian, Energetic spanwise modes in the logarithmic layer of a turbulent boundary layer, J. Fluid Mech. **545**, 141 (2005).
[43] J. C. del Álamo and J. Jiménez, Spectra of the very large anisotropic scales in turbulent channels, Phys. Fluids **15**, L41 (2003).
[44] C. M. de Silva, D. Chandran, R. Baidya, N. Hutchins, and I. Marusic, Periodicity of large-scale coherence in turbulent boundary layers, Int. J. Heat Fluid Flow **83**, 108575 (2020).
[45] J. Zhou, R. J. Adrian, and S Balachandar, Autogeneration of near-wall vortical structures in channel flow, Phys. Fluids **8**, 288 (1996).
[46] J. Zhou, R. J. Adrian, S. Balachandar, and T. M. Kendall, Mechanisms for generating coherent packets of hairpin vortices in channel flow, J. Fluid Mech. **387**, 353 (1999).
[47] R. J. Adrian, C. D. Meinhart, and C. D. Tomkins, Vortex organization in the outer region of the turbulent boundary layer, J. Fluid Mech. **422**, 1 (2000).
[48] D. J. C. Dennis and T. B. Nickels, Experimental measurement of large-scale three-dimensional structures in a turbulent boundary layer. Part 1. Vortex packets, J. Fluid Mech. **673**, 180 (2011).
[49] J. P. Monty, D. Chandran, R. Baidya, and I. Marusic, Measurements of the two-dimensional energy spectra of wall-turbulence at high Reynolds number, in *TSFP Digital Library Online* (Begel House, Chicago, USA, 2017).

[50] K. C. Kim and R. J. Adrian, Very large-scale motion in the outer layer, Phys. Fluids **11**, 417 (1999).
[51] A. E. Perry and I. Marusic, A wall-wake model for the turbulence structure of boundary layers. Part 1. Extension of the attached eddy hypothesis, J. Fluid Mech. **298**, 361 (1995).
[52] Y. Jodai and G. E. Elsinga, Experimental observation of hairpin auto-generation events in a turbulent boundary layer, J. Fluid Mech. **795**, 611 (2016).
[53] J. H. Lee, Evolution of Canonical Turbulent Boundary Layers, Ph.D. thesis, The University of Melbourne (2017).
[54] M. H. Buschmann, T. Indinger, and M. Gad-el Hak, Near-wall behavior of turbulent wall-bounded flows, Int. J. Heat Fluid Flow **30**, 993 (2009).
[55] J. P. Monty and M. S. Chong, Turbulent channel flow: Comparison of streamwise velocity data from experiments and direct numerical simulation, J. Fluid Mech. **633**, 461 (2009).
[56] M. Vallikivi, B. Ganapathisubramani, and A. J. Smits, Spectral scaling in boundary layers and pipes at very high Reynolds numbers, J. Fluid Mech. **771**, 303 (2015).
[57] M. Lee and R. D. Moser, Direct numerical simulation of turbulent channel flow up to $\mathrm{Re}_\tau = 5200$, J. Fluid Mech. **774**, 395 (2015).
[58] J. Jiménez and S. Hoyas, Turbulent fluctuations above the buffer layer of wall-bounded flows, J. Fluid Mech. **611**, 215 (2008).
[59] X. I. A. Yang, C. Meneveau, I. Marusic, and L. Biferale, Extended self-similarity in moment-generating-functions in wall-bounded turbulence at high Reynolds number, Phys. Rev. Fluids **1**, 044405 (2016).
[60] M. Vallikivi, M. Hultmark, and A. J. Smits, Turbulent boundary layer statistics at very high Reynolds number, J. Fluid Mech. **779**, 371 (2015).